Astron. Astrophys. 320, 612–619 (1997)

ASTRONOMY
AND
ASTROPHYSICS

Electron acceleration sites in a large-scale coronal structure

K.-L. Klein[1], **H. Aurass**[2], **I. Soru-Escaut**[1], **and B. Kálmán**[3]

[1] DASOP, CNRS-URA 2080, Observatoire de Paris, Section de Meudon, F-92195 Meudon, France (klein@obspm.fr)
[2] Astrophysikalisches Institut Potsdam, Observatorium für solare Radioastronomie, Telegrafenberg A31, D-14473 Potsdam, Germany (haurass@aip.de)
[3] Heliophysical Observatory of the Hungarian Academy of Sciences, P.O. Box 30, Debrecen, Hungary (kalman@tigris.klte.hu)

Received 25 June 1996 / Accepted 21 August 1996

Abstract. Radio observations and interplanetary particle measurements have shown that even in the absence of conspicuous violent processes in the low atmosphere (such as H_α flares) electrons are accelerated in the corona, most likely at higher altitudes than during flares ($\geq$0.5 $R_\odot$ above the photosphere). The paper presents direct evidence on the acceleration sites from a case study of radio, visible light and soft X-ray observations: electrons are repeatedly accelerated in a large-scale coronal structure which is identified with a streamer in coronographic observations. Energy is simultaneously released in an active region near the base of the structure and at a height of $\sim$1 $R_\odot$, over several hours before the large-scale structure erupts. Energy input is observed in at least two emerging active regions underneath the streamer. The coronal configuration is three-dimensional, overlying a whole quadrant of the Sun. It is argued that the observations trace multiple sites of energy release presumably in current sheets embedded within the streamer, in agreement with scenarios developed for the acceleration of electrons seen in the corona and at 1 AU, and for the evolution of large-scale coronal structures towards eruption.

Key words: Sun: corona – Sun: flares – Sun: magnetic field – Sun: particle emission – Sun: radio radiation – acceleration of particles

1. Introduction

Suprathermal electron populations are a characteristic signature of energy release associated with active regions on the Sun. The structures where, and the mechanisms by which, particles are energized have not yet been identified. Although the bulk of the nonthermal particles seen during flares is accelerated at low heights ($\sim 10^4$ km; cf. Lin 1993; Klein 1994 and references therein), there seems to be significant acceleration at least of low-energy electrons at altitudes $\sim 2\cdot10^5$ km (Kane et al. 1992). Coronal acceleration above active regions is inferred from noise storm observations outside flares (e.g. Raulin & Klein 1994; Crosby et al. 1996). The most frequent interplanetary electron events, beams up to 15 keV ("impulsive electron events"), must be accelerated at heights above 0.5 $R_\odot$ because otherwise their spectrum would have a low-energy cutoff at several keV which is not observed (Potter et al. 1980; Lin 1985, 1993).

The paper presents observational constraints on coronal sites of electron acceleration, using spectrographic and imaging observations of fast-drift bursts. Bursts of type III, drifting in the frequency-time plane from high to low frequencies, and those with reversed sense of drift (III-RS or RS - reverse slope) are due to electron beams. The sense of the drift indicates whether the beams travel towards lower densities (type III) or towards higher densities (RS). Reviews on fast-drift bursts were given by Goldman & Smith (1985), Suzuki & Dulk (1985) and Pick & van den Oord (1990).

The outline of the paper is as follows: The instrumentation is briefly described in Sect. 2. Spectral and imaging observations of groups of fast-drift bursts are given in Sect. 3.1. The observed sites of emission are compared with features seen in visible light in Sect. 3.2. Section 3.3 shows that the radio bursts are associated with soft X-ray brightenings. The bulk of observations is suggestive of co-ordinated energy release at different sites within a coronal streamer which evolves under the influence of magnetic flux emergence underneath its span (Sect. 3.4). The results are discussed in Sect. 4.

A preliminary analysis was given by Klein & Aurass (1993).

2. Instruments

The observations were carried out at radio wavelengths with the spectrograph of the Tremsdorf Solar Radio Observatory (OSRA) and the Nançay Radioheliograph (NRH), and in the H_α line with the 3-λ Heliograph in Meudon. The OSRA instrument consists of swept-frequency spectrographs in the ranges 40–90, 100–170, 200–400 and 400–800 MHz, with a sweep rate of 10 s^{-1}, and of a grid of single frequency receivers in the same spectral range (Mann et al. 1992). At the time of the observations

Send offprint requests to: K.-L. Klein

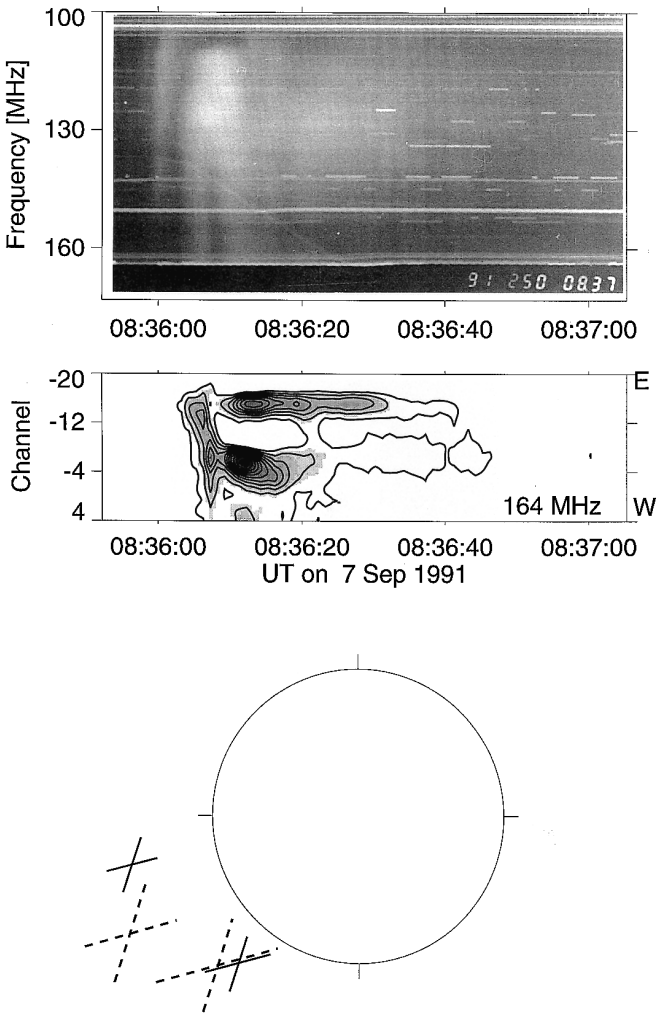

Fig. 1. Spectrographic and heliographic data during a group of fast-drift bursts. Top: Dynamic spectrum. Middle: One-dimensional brightness distribution (integrated in the direction perpendicular to the array). Vertical axis: position projected onto the terrestrial east-west direction, from the eastern (channel -32) to the western border (channel 31) of the field of view, centre of the photospheric disk in channel 0. Linear contours from 4.3% to 100% of maximum brightness in the plotted field (steps of 8.7%). Bottom: Location and half-power diameter of the two reverse-drift bursts (164 MHz) at 8:36:05-8:36:07 (dashed) and 8:36:12-8:36:13 UT (solid). North is on top, east to the left.

used here, the dynamic spectrograms were recorded on film. The NRH provides one-dimensional scans of the corona at five frequencies, with both its east-west and north-south branches (The Radioheliograph Group 1993). The instrument was used in a preliminary version, with 16 interferometers in the east-west direction, spanning baselines from 100 to 1600 m, and the complete 23 element array in the north-south direction. The integration time was 1 s. The NRH observed at 164, 236.6, 327, 408 and 435 MHz. The 3-λ Heliograph takes one image of the Sun per minute in the centre and both wings ($\pm$0.5 Å) of the H_α line.

3. The observations

3.1. Groups of fast-drift radio bursts on 7 September 1991

Several fast-drift bursts were observed by the Tremsdorf spectrograph and the Nançay Radioheliograph between 8 and 12 UT. Figs. 1 and 2 display observations of the two most prominent groups in the range 100–170 MHz, comprising bursts with ordinary drift (from high to low frequencies; type III) and reverse drift (RS). These groups precede a filament eruption that starts at 11:40 UT. The bursts are in general not continuous across the observed spectral band: Most of the clearly identified type III bursts start near or above 300 MHz and end somewhere in the unobserved range between 170 and 200 MHz. The RS bursts have their high-frequency cutoff in this range. They can be followed down to 110–130 MHz. RS bursts in the range 170–130 MHz occur together with type III bursts in the band 200–400 MHz.

During the first group (Fig. 1) the most prominent feature in the dynamic spectrum is a pair of bursts with reversed drift above 130 MHz. It is preceded by a type J burst starting near 150 MHz with low-frequency turnover at 75 MHz (i.e. below the lowest frequency shown in the spectrum). Below 130 MHz the RS bursts merge into a single structure that drifts towards lower frequencies and is sharply cut off near 108 MHz. Broadband emission follows, predominantly below 150 MHz.

The temporal evolution of radio sources at 164 MHz as seen by the NRH is displayed in the middle line of Fig. 1 as a contour and gray-scale plot of equal brightness in a space-time plane. The vertical axis gives the position projected on the terrestrial east-west direction. The pair of RS bursts is clearly identified: the first one between 8:36:05 and 8:36:08 UT, the second starting 8:36:10 UT. The remarkable feature here is that during both bursts two sources brighten nearly simultaneously at different places. Their heliographic positions and sizes are plotted as crosses in Fig. 1 (bottom). The sources of the first RS burst are given by dashed crosses (distance between the two sources: 0.7 $R_\odot$). During the second RS burst the sources (solid crosses) have larger distance (0.9 $R_\odot$) and lower projected height. At 164 MHz weak emission continues from the north-eastern site until about 8:38:15 UT. Due to its weakness its spectral identification is uncertain.

The second strong burst group (Fig. 2) consists of type III bursts before 10:46:40 UT, and of weak type III bursts and three prominent bursts with reversed slope afterwards. Like in the preceding group, the reverse drift bursts are connected at frequencies below 130 MHz by a negatively drifting emission with well-defined low-frequency cutoff.

Different source configurations are observed before and after 10:46:40 UT. The initial type III bursts come from two neighbouring sites above the eastern limb (dashed crosses in the bottom panel of Fig. 2). The easternmost (i.e. higher) source is the brighter one. The type III bursts seen above 200 MHz are also emitted above the eastern limb. During the subsequent RS bursts the source geometry is more complex. The former type III sources brighten again. Like in the 8:36 UT group, two nearly simultaneous sources with comparable brightness are ob-

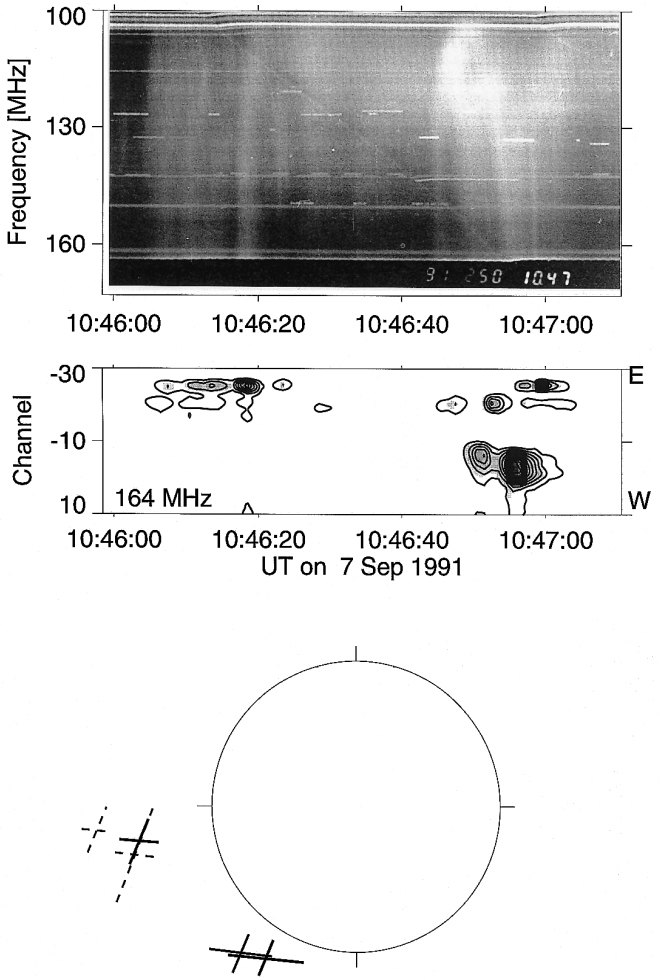

Fig. 2. Similar to Fig. 1, for the second group of fast-drift bursts on 7 Sep 1991. The dashed crosses in the bottom panel refer to the sources of type III bursts, solid crosses to the north-eastern branch of the RS-burst at 10:46:53 UT and the two south-western RS sources at 10:46:52 and 10:46:56 UT.

served during the RS-burst emission (solid crosses). Two successive bursts occur in the south-western source. The second burst is slightly west of the first one. Subsequently both the north-eastern and the south-western source brighten again, but are too weak for spectral identification. Emission at 164 (and 236 MHz) ceases near 10:47:45 UT.

The third prominent group of type III bursts occurs at 10:58 UT (10:58:20 – 10:59 at 164 MHz). It displays the same two-component source configuration as the type III bursts at 10:46 UT. No reverse-drift bursts are identified in the spectrum, and the south-western source complex observed at 8:36 and 10:46:40 UT does not appear during this group.

In summary, the type III bursts are located above the eastern limb. Like in many other cases their emission involves more than one simple source (Raoult & Pick 1980; Pick & Ji 1987). Reverse-slope bursts come from two quasi-simultaneous sources which are farther apart from each other than individual type III sources: one component is close to the type III bursts, while the second one is at a distance up to nearly 1 $R_\odot$ above the south-eastern limb.

The reverse-slope bursts are not the descending branches of type U bursts: the only drift visible above 130 MHz during the strong bursts in the periods 8:36:04 - 8:36:15 UT and 10:46:40 – 10:47:00 UT is towards higher frequencies. In the 8:36 UT group these bursts are clearly separated in the spectrum from the preceding type J burst which extends to lower frequencies.

In both groups there is a smooth transition between reverse drift above 130 MHz and ordinary drift below. This indicates that acceleration occurs around a region where the electron density is $2 \cdot 10^8$ cm^{-3} or $5 \cdot 10^7$ cm^{-3}, depending on whether the emission is fundamental or harmonic.

3.2. Radio source positions and visible light features

In Fig. 3 the positions and sizes of all 164 MHz sources during the three burst groups are plotted upon the daily image of the Mark 3 Mauna Loa coronameter taken on 6 Sep 1991 at 18:03 UT, i.e. 14 to 17 hours before the radio events. The daily Meudon H_α spectroheliogram (7 Sep 1991) is inserted. The locations and NOAA numbers of relevant active regions are given in the schematic drawing on the right, together with the contours of a coronal hole observed in the He I 10830 Å line (Kitt Peak).

The southern complex of radio sources is located above an old active region (NOAA 6817) with a single spot surrounded by a filament. The northern source complex lies above an active region at the limb (NOAA 6822). South of it, AR 6824 crosses the limb on 8 Sep. Two active regions are emerging north-west and north-east of AR 6817. This complex is bordered on its western side by a coronal hole which extends from the south pole to the northern hemisphere.

The two simultaneously observed sources during the reverse-slope bursts (solid crosses) project in general onto opposite sides of a bright white-light feature. By its altitude (emission seen up to 1.3 $R_\odot$ above the limb) this feature is to be regarded as a streamer, although the typical cusp shape known from eclipse photographs is not seen in the coronographic image (Sime & McCabe 1990). In one case (8:36:04 UT) one of the two radio sources projects close to the top of the mound-shaped bright inner region of the streamer. The type III sources (dashed crosses) project onto the gap between this streamer and the neighbouring feature to the north.

The association of radio sources with the white-light streamer does not critically depend on the day of the coronographic observations. The same result as in Fig. 3 is obtained with the following available Mauna Loa daily image on 8 Sep 1991. The same basic configuration is seen above the eastern and south-eastern limb, with the only difference that the gap between the two white-light structures is partly filled in. We therefore consider that the radio sources are located in a three-dimensional streamer configuration extending from east of the coronal hole to behind the eastern limb.

Fig. 3. Image of the white-light corona taken with the Mauna Loa K-coronameter on 6 Sep 1991 (Courtesy High Altitude Observatory, National Center for Atmospheric Research (NCAR), Boulder, Colorado, USA) together with the positions and sizes of 164 MHz sources of the fast-drift bursts occurring in three groups during the morning of 7 Sep. Dashed crosses: type III bursts, solid crosses: reverse-slope bursts. The white-light image is a weighted average of 36 data sets. The Meudon H_α spectroheliogram (7 Sep, 6:22 UT) is inserted. The schematic drawing on the top right gives the locations (squares) and NOAA numbers of relevant active regions and the outline (shaded region) of a coronal hole seen in the Kitt Peak He I 10830 Å observations (adapted from NOAA-SESC 1991).

The RS bursts from the south-western border of the streamer are not all emitted at the same site. Figs. 1 (e.g. 8:36:10–8:36:20 UT) and 2 show that in both groups the later RS emission comes from a source displaced westward from the first RS burst, yielding an apparent westward movement of the brightest feature during a few seconds. The white light picture shows that this apparent movement is directed towards outer and lower layers of the streamer. It is plausible that if electron beams are injected over a prolonged duration (several seconds) onto different field lines in the high corona, the later 164 MHz emission will come from regions of the streamer farther away from its centre, where the appropriate plasma level is at lower altitude.

3.3. Soft X-ray emission and search for H_α features

Fig. 4 (left column) compares the radio emission at 164 MHz on 7 Sep 1991 with the X-ray fluxes detected by the GOES full Sun monitors (courtesy Solar Data Analysis Center at GSFC). The time intervals of H_α flares reported in *Solar Geophysical Data* (henceforth SGD) 571-II are given by horizontal bars, together with the location on the Sun. The three strongest groups of fast-drift bursts are seen as short brightness enhancements at 8:36, 10:46 and 10:58 UT. After 12 UT a moving type IV burst is observed which has been briefly analysed elsewhere (The Radioheliograph Group 1993, Fig. 3). It occurs together with the eruption of the filament around AR 6817 (cf. Fig. 3). Although this eruption is not the main topic of the present study, we shall come back to it in Sect. 4.3.

The brightest X-ray events before 12 UT are associated with H_α flares in the western hemisphere (including the fading emission at the beginning of the time interval plotted in Fig. 4). They have no metric radio counterpart. On the other hand, at the times of the three groups of fast drift bursts, impulsive soft X-ray brightenings occur superposed upon the declining emission from the well-identified flares. The time histories of the X-ray fluxes during the individual events are plotted together with their derivatives (dashed line) in the right column of Fig. 4. The duration of the fast-drift bursts at 164 MHz is indicated by a horizontal bar at the bottom of each plot. During the first two burst groups the radio emission persists as long as the derivative of the soft X-ray flux is positive, i.e. as long as the X-ray source is heated. This suggests a physical link between energy release to the soft X-ray plasma and electron beam production (cf. Sect. 4), similar to the well-known relationship between impulsive microwave or hard X-ray bursts with soft X-ray events (Neupert 1968; Dennis & Zarro 1993). During the third burst group the metric emission occurs only at the onset of the heat input into the X-ray plasma.

The peak fluxes of these X-ray brightenings, after subtraction of the pre-event emission, range from $5{\cdot}10^{-7}$ to $10{\cdot}10^{-7}$ Wm^{-2} in the 1-8 Å channel. Given a background level of about $5{\cdot}10^{-7}$ Wm^{-2}during quiescent periods in September 1991 (cf. SGD 571-II), the events are of class C1 in the GOES classification. A rough estimation using the method of Thomas et al. (1985) and the GOES detector efficiencies given by Sylwester et al. (1995) yields isothermal temperatures slightly above 10^7 K in the soft X-ray emitting plasma.

Where do the X-ray bursts occur ? Since no flares were reported at those times, weak H_α signatures have been searched for in the observations of the Meudon $3-\lambda$ Heliograph. While there is continuing activity in filaments and prominences, no specific feature coincides in time with the fast-drift bursts (contrary to LaBonte (1976) and Tang & Moore (1982)). We therefore suppose that the emission is occulted and that the X-ray brightenings occur on or behind the limb, probably in AR 6822 which is at the right latitude to account for the type III bursts (cf. Fig. 3).

3.4. Gradual evolution of the large-scale coronal structure

The coronal structure inferred from the radio and white light observations overlies several active regions (Fig. 3). Their evolution before and after 7 Sep is displayed in the series of daily Meudon spectroheliograms (Fig. 5), and analyzed with more detail in the Debrecen white-light observations. AR 6817 does not show any sign of evolution, and no rotational motion of the spot is observed. However, AR 6820 and 6823 are emerging

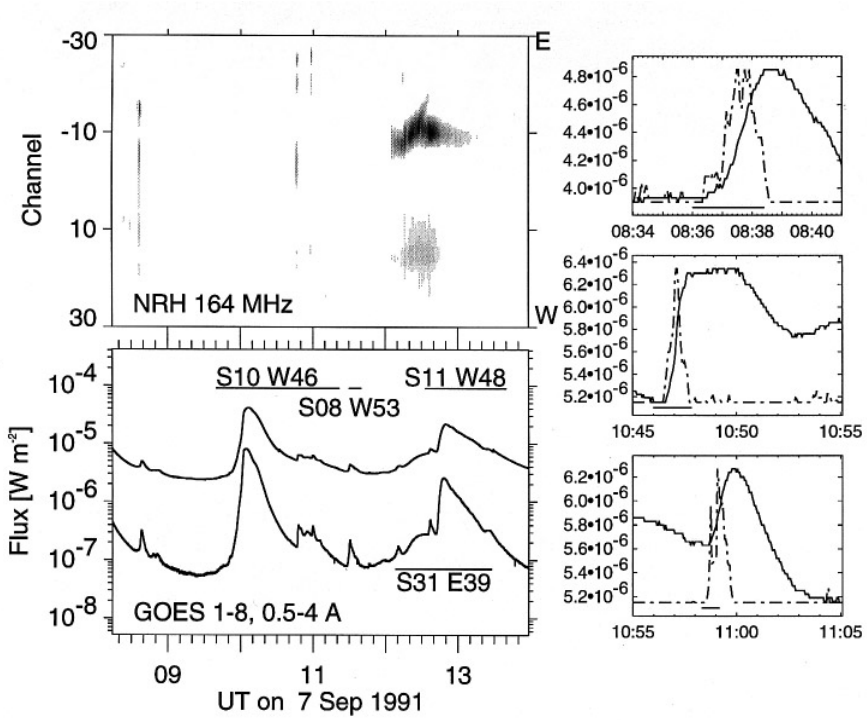

Fig. 4. Left column: Comparison of 164 MHz emission with whole-Sun soft X-ray fluxes in the ranges 1-8 Å (top) and 0.5-4 Å (bottom). The 164 MHz brightness distribution seen by the east-west branch of the NRH is given in gray levels from 4.3% to 100% of maximum brightness in the field. The centre of the photospheric disk is at channel 0, the width of the field varies from 1.4° at 8:30 UT to 1° at noon (11:49 UT). Apparently enhanced emission in the lower half of the plot is due to sidelobes and baseline distortions. Right column: Time history of the soft X-ray flux (0.5-4 Å; solid line) and its derivative (dashed line) during three events occurring together with the metric fast-drift bursts. Only positive values of the derivative are plotted to trace the energy supply to the X-ray source, while negative and zero values are confined to the constant baseline. The units on the vertical axis refer to the flux. The derivative has been scaled so as to fit into the same plot. The duration of the 164 MHz burst groups is indicated by horizontal bars underneath the soft X-ray curves.

and forming pores, then spots, between 6 Sep and 10 Sep. The evolution is quick in the following part of AR 6820, where spots develop earlier than in the leading part. This leads to the gradual re-configuration of the large-scale coronal magnetic field witnessed by the progressive separation of the coronal hole at the place where AR 6820 emerges (NOAA-SESC 1991; cf. Fig. 3). H_α flare activity started not earlier than 23:20 UT on 7 Sep in these evolving regions, and was restricted to a few subflares. The episodes of energy release discussed here are probably part of the process by which the coronal structure adjusts itself to the changing boundary conditions in the lower atmosphere, up to the time when a more abrupt re-arrangement leads to the eruption of the filament in AR 6817 (starting 7 Sep 1991, 11:40 UT) and to the moving type IV burst.

4. Discussion

During several episodes on 7 Sep 1991 electron beams have been observed to come from different acceleration sites: upward travelling beams producing metric type III bursts from an active region, and downward travelling beams that emit III-RS bursts from a region about 1 $R_\odot$ above the photosphere. The pairwise brightening of the radio sources during the RS bursts suggests one of the following scenarios for acceleration at 1 $R_\odot$ above the photosphere:

1. beam injection into opposite directions along closed field lines which connect widely separated regions in the underlying atmosphere,
2. downward injection onto field lines which are close to each other near the acceleration site, but separate in the underlying atmosphere.

It is generally believed that the large-scale structure of coronal streamers contains closed magnetic flux surrounded by field lines opened towards interplanetary space by the solar wind, and that current sheets separate open and closed magnetic fluxes in the low corona and oppositely directed open field lines in the high corona (e.g. Pneuman & Orrall 1986; Koutchmy & Livshits 1992). Current sheets play a prominent role in models of coronal energy release (cf. reviews by van den Oord 1993, Kliem 1995). They are possible sites for electron acceleration in both configurations cited above, either at the interface between open and closed magnetic flux in the lower part of the streamer (1) or those which separate oppositely directed field lines in the "stalk" (2). This scenario is corroborated by the projected location of the radio sources on opposite sides of a white-light feature observed with the HAO Mk3 K-coronameter.

Jet-like structures in coronographic images have been shown earlier to guide electron beams to the high corona (Trottet et al. 1982), and decametric type III bursts were observed in the stalk of coronal streamers (Kundu et al. 1983). The present observations complete these findings, and give more direct evidence on the sites of beam production. Current sheets within helmet streamers have been considered as the accelerators of electrons emitting metric noise storms and escaping towards interplanetary space (Gubchenko & Zaitsev 1983). Cliver & Kahler (1991) used such a scenario to discuss the origin of interplanetary electron beams observed without chromospheric signatures. The same global configuration, although on smaller spatial scale,

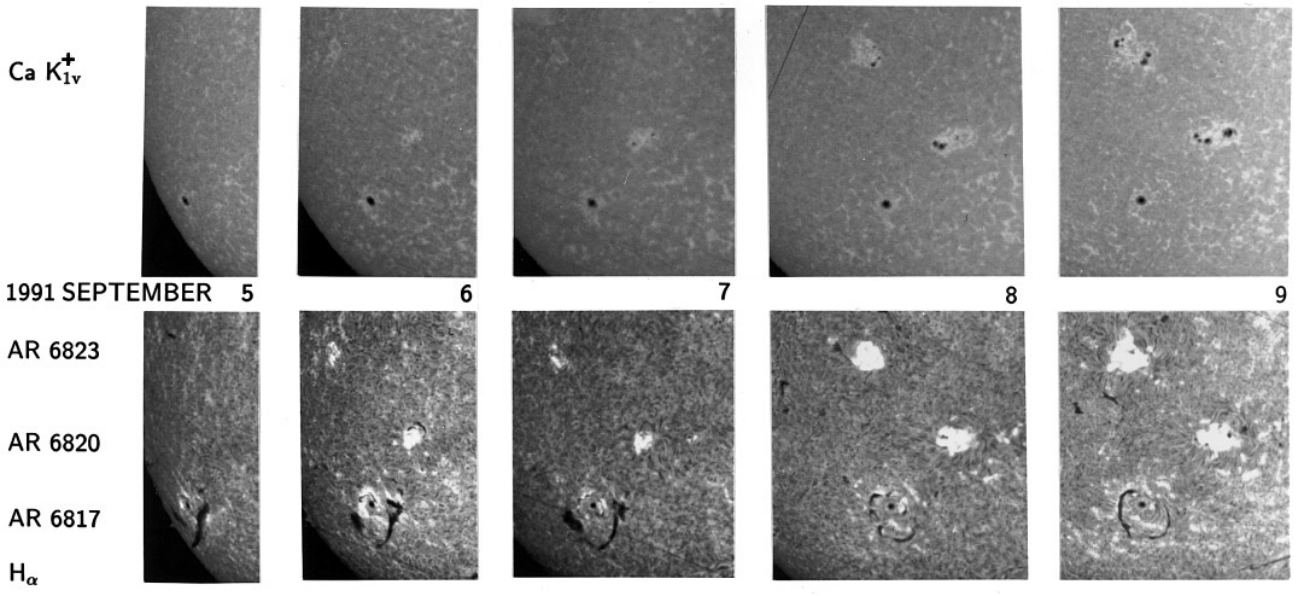

Fig. 5. Day-to-day evolution of the active regions in the south-eastern solar quadrant, observed from 5 to 9 Sep 1991 in Ca II K $_{1v}$ (upper row) and in H_α (lower row; Meudon spectroheliograph). The NOAA numbers of the active regions are given at the appropriate latitude in the left margin.

has recently been used to explain the topology of coronal hard X-ray sources (Masuda et al. 1995).

4.1. Relationship between electron beams and soft X-ray brightenings

The high coronal acceleration is not an isolated phenomenon within the large-scale structure. Type III bursts due to electron beams produced at lower altitudes are observed within the same groups. The observed one-to-one correspondence between X-ray brightenings and groups of fast drift bursts, in particular the similar duration of beam production and heating, show a physical relationship between both processes. The joint production of X-ray brightenings and type III emitting electron beams is a frequent simultaneous manifestation of energy release in an active region (e.g. Aurass et al. 1994; Raulin et al. 1996). Raulin et al. (their Fig. 1) show a group of type III bursts during the rising phase of soft X-ray emission from a jet, with the same relative timing of the soft X-ray flux and the radio emission as in Fig. 4. The relationship of X-ray brightenings and type III bursts with electron acceleration at 1 $R_\odot$ above the photosphere is less obvious. The beams emitting the RS bursts do not penetrate to below the level of 200 MHz, i.e. to plasma layers denser than $\sim 10^8$ cm^{-3}, presumably because they are deflected by the convergence of the magnetic field and by Coulomb collisions (e.g. Krucker et al. 1995, Fig. 8). Furthermore, energy input into the X-ray plasma is in all three events accompanied by type III bursts, but not always by RS bursts (e.g., during the 10:46 and 10:58 UT groups). The observations therefore suggest that co-ordinated episodes of energy release are triggered at different sites within the large-scale coronal structure. Given the joint occurrence of RS bursts and type III bursts within about 10 s, the trigger of the electron acceleration at 1 $R_\odot$ must propagate at a typical particle velocity (of the order of $0.1 R_\odot$ s^{-1}), rather than at an MHD velocity.

4.2. Coronal acceleration of electron beams observed at 1 AU

The scenario of co-ordinated episodes of energy release at widely separated altitudes allows also for the simultaneous production of electrons escaping towards interplanetary space (Cliver & Kahler 1991). The density of the high acceleration region was inferred above to be $5 \cdot 10^7$ cm^{-3} or $2 \cdot 10^8$ cm^{-3}, depending on the mode of radio emission. The lower value is about twice the electron density derived from white-light observations of streamers at 1 $R_\odot$ above the photosphere (cf. Koutchmy & Livshits 1992, Fig. 6), and 3 times higher than the density extrapolated from the interplanetary density distribution derived by Fainberg & Stone (1974) and used by Lin (1985) in his model calculations of electron spectra. We recall that the radio diagnostics provide a direct measurement of the local electron density, whilst the white-light data give the average density along the line of sight. If the electron density inferred from our radio measurements is relevant to the acceleration site, Coulomb losses are more efficient than supposed in Lin's computations, and the acceleration will occur above 1 $R_\odot$. But the present observations confirm the streamer scenarios of high coronal acceleration and provide evidence that this is part of the gradual evolution of streamers which may ultimately lead to major events of magnetic field reconfiguration. Given the co-operative energy release at different altitudes evidenced by the present observations, there is no reason to believe that acceleration sites do not exist at still greater altitudes, since

a highly filamentary structure of streamers is observed far into the interplanetary space (Woo et al. 1995).

4.3. Destabilisation of large-scale coronal structures

The passive role of large-scale coronal structures in channelling particles over large distances has been demonstrated earlier (e.g. Kai 1969; Simnett 1982; Nakajima et al. 1985; cf. review by Simnett 1993; Willson et al. 1993; Aurass & Klein 1996). In addition to electron acceleration the present observations trace the evolution of a large-scale coronal structure towards a major reconfiguration. The radio, X-ray and visible light observations illustrate the evolution which Bruzek (1952) and Feynman and Martin (1995) argued to be typical for the destabilisation of filaments in the course of magnetic flux emergence under their span or in their vicinity, as well as the streamer - interconnection of active regions of different age at different latitudes eventually leading to a coronal mass ejection (Kahler 1991). The widely separated coronal activities on 7 Sep 1991 witness instabilities in the large-scale structure during a few hours before it erupts. They outline the relation of gradual evolution towards eruption and increased production of electron beams found by Jackson & Sheridan (1979). Wild (1968) showed imaging observations of another event which can only be explained by energy release at great height in the corona. The combination of spectral and imaging observations of the 7 Sep 1991 burst groups provides new evidence for this. A systematic search for the origin of metric reverse-slope bursts as tracers of coronal instabilities is necessary.

5. Conclusions

The key results of the present analysis are summarized as follows:

1. Electron beams are produced near one footpoint and at 1 $R_\odot$ above the photosphere in a large-scale coronal structure which appears as a streamer in coronographic observations. Beam production and plasma heating occur simultaneously and repeatedly during several hours.
2. The radio source configuration is consistent with beam production in the current sheets separating regions of open and closed magnetic flux near the base of the streamer and oppositely directed field lines above its cusp. This is the direct confirmation of scenarios devised earlier for the acceleration of low-energy electron events observed at 1 AU.
3. Since beam production at the two widely separated sites occurs within the same burst groups with about 1 min duration each, the trigger must propagate at a typical particle speed, rather than the Alfvén speed.
4. The large-scale structure overlies several active regions covering a whole quadrant in the photosphere. Magnetic flux emergence observed in two of them is the likely energy source. It ultimately drives the coronal structure towards eruption, as suggested by previous statistical studies.

Acknowledgements. The authors are grateful to the generous supply of Mauna Loa white-light images by HAO/NCAR (NCAR is sponsored by the National Science Foundation) and of GOES soft X-ray observations by the NASA/GSFC Solar Data Analysis Center. They thank their colleagues running the daily observations at Potsdam - Tremsdorf, Nançay, Meudon and Debrecen. They acknowledge discussions with Drs. Ø. Elgarøy, M. Karlicky, A. Klassen, R.P. Lin, G. Mann, J.C. Noëns and G. Trottet. We thank Mrs A. Lecinski, Mr D. Scholz and Mr G. Servajean for preparing illustrations. The Nançay Radio Observatory is funded by the French Ministry of Education, the CNRS and the Région Centre. This paper became possible due to travel grants 312/pro-bmft-gg (DAAD) and 94053 (MAE) within the German-French PROCOPE programme.

References

Aurass H., Klein K.-L., 1996, A&AS, in press
Aurass H., Klein K.-L., Martens P.C.H., 1994, Sol. Phys. 155, 203
Bruzek A., 1952, Z. Astrophys. 31, 99
Cliver E., Kahler S., 1991, ApJ 366, L91
Crosby N., Vilmer N., Lund N., Klein K.-L., Sunyaev R., 1996, Sol. Phys. 167, 333
Dennis B.R., Zarro D. M., 1993, Sol. Phys. 146, 177
Fainberg J., Stone R.G., 1974, Spa. Sci. Rev. 16, 145
Feynman J., Martin S.F., 1995, JGR 100, 3355
Goldman M.V., Smith D.F., 1985, in Sturrock P.A. (ed.) Physics of the Sun, Vol. II, Reidel, Dordrecht, p. 325
Gubchenko V.M., Zaitsev V.V., 1983, Sol. Phys. 89, 391
Jackson B.V., Sheridan K.V., 1979, PASA 3, 383
Kahler S., 1991, ApJ 378, 398
Kai K., 1969, PASA 1, 186
Kane S.R., McTiernan J., Loran J., Fenimore E.E., Klebesadel R.W., Laros J.G., 1992, ApJ 390, 687
Klein K.-L., 1994, in Belvedere G., Rodonó M., Simnett G.M. (eds.), Advances in Solar Physics, Lecture Notes in Physics 432, Springer, p. 261
Klein K.-L., Aurass H., 1993, Adv. Space. Res. 13(9), 295
Kliem B., 1995, in Benz A.O., Krüger A. (eds.), Coronal Magnetic Energy Relases, Lecture Notes in Physics 444, Springer, p. 93
Koutchmy S., Livshits M., 1992, Spa. Sci. Rev. 61, 393
Krucker S., Aschwanden M.J., Bastian T.S., Benz A.O., 1995, A&A 302, 551
Kundu M.R., Gergely T.E., Turner P.J., Howard R.A., 1993, ApJ 269, L67
LaBonte B.J., 1976, Sol. Phys. 50, 201
Lin R.P., 1985, Sol. Phys. 100, 537
Lin R.P., 1993, Adv. Space. Res. 13(9), 265
Mann G., Aurass H., Voigt W., Paschke J., 1992, in Coronal Streamers, Coronal Loops and Coronal and Solar Wind Composition, ESA SP-348, 129
Masuda S., Kosugi T., Hara H., Sakao T., Shibata K., Tsuneta S., 1995, PASJ 47, 677
Nakajima H., Dennis B.R., Hoyng P., Nelson G., Kosugi T., Kai K., 1985, ApJ 288, 806
Neupert W.M., 1968, ApJ 153, L59
NOAA-SESC, 1991, Prelim. Rep. and Forecast of Solar Geophys. Data, SESC-PRF 836
Pick M., Ji S.-C., 1986, Sol. Phys. 107, 159
Pick M., van den Oord G.H.J., 1990, Sol. Phys. 130, 83
Pneuman G.W., Orrall F.Q., 1986, in Sturrock P.A. (ed.), Physics of the Sun, Vol. II, Reidel, Dordrecht, p. 71

Potter D.W., Lin R.P., Anderson K.A., 1980, ApJ 236, L97
The Radioheliograph Group 1993, Adv. Space Res. 13(9), 411
Raulin J.P., Klein K.-L., 1994, A&A 281, 536
Raulin J.P., Kundu M.R., Hudson H.S., Nitta N., Raoult A., 1996, A&A 306, 299
Raoult A., Pick M., 1980, A&A 87, 63
Sime D.G., McCabe M.K., 1990, Sol. Phys. 126, 267
Simnett G.M., 1982, ApJ 255, 721
Simnett G.M., 1993, Adv. Space Res. 13(9), 133
Suzuki S., Dulk G.A., 1985, in McLean D.J., Labrum N.R. (eds.), Solar Radiophysics. Cambridge University Press, Cambridge, p. 289
Sylwester J., Garcia H.A., Sylwester B., 1995, A&A 293, 577
Tang F., Moore R.L., 1982, Sol. Phys. 77, 263
Thomas R.N., Starr R., Crannell C.J., 1985, Sol. Phys. 95, 329
Trottet G., Pick M., House L., Illing R., Sawyer C., Wagner W., 1982, A&A 111, 306
van den Oord G.H.J., 1993, Adv. Space Res. 13(9), 143
Wild J.P., 1968, PASA 1, 136
Willson R.F., Lang K.R., Gary D.E., 1993, ApJ 418, 490
Woo R.T., Armstrong J.W., Bird M.K., Pätzold M., 1995, ApJ 449, L91

This article was processed by the author using Springer-Verlag LaTeX A&A style file *L-AA* version 3.